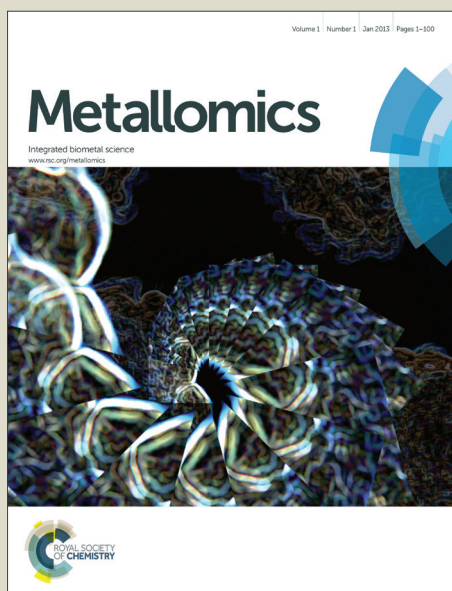


# Metallomics

Accepted Manuscript



This is an *Accepted Manuscript*, which has been through the Royal Society of Chemistry peer review process and has been accepted for publication.

*Accepted Manuscripts* are published online shortly after acceptance, before technical editing, formatting and proof reading. Using this free service, authors can make their results available to the community, in citable form, before we publish the edited article. We will replace this *Accepted Manuscript* with the edited and formatted *Advance Article* as soon as it is available.

You can find more information about *Accepted Manuscripts* in the [Information for Authors](#).

Please note that technical editing may introduce minor changes to the text and/or graphics, which may alter content. The journal's standard [Terms & Conditions](#) and the [Ethical guidelines](#) still apply. In no event shall the Royal Society of Chemistry be held responsible for any errors or omissions in this *Accepted Manuscript* or any consequences arising from the use of any information it contains.

## ARTICLE

# Quantitation and localization of intracellular redox active metals by X-ray fluorescence microscopy in cortical neurons derived from APP and APLP2 knockout tissue

Cite this: DOI: 10.1039/x0xx00000x

Received 30th June 2014,

Accepted

DOI:

www.rsc.org/

Giuseppe D. Ciccotosto<sup>a\*</sup>, Simon A. James<sup>b,c</sup>, Matteo Altissimo<sup>d</sup>, David Paterson<sup>b</sup>, Stefan Vogt<sup>e</sup> Barry Lai<sup>c</sup>, Martin D. de Jonge<sup>b</sup>, Daryl L. Howard<sup>b</sup>, Ashley I. Bush<sup>f</sup> and Roberto Cappai<sup>a</sup>

The amyloid precursor protein (APP) gene family includes APP and the amyloid precursor-like proteins, APLP1 and APLP2. These proteins contain metal binding sites for copper, zinc and iron and are known to have physiological roles in modulating the metal homeostasis in brain cells. Here we report the application of X-ray fluorescence microscopy (XFM) to investigate the subcellular distribution patterns of the metal ions Cu, Zn, Fe, and Ca in individual neurons derived from APP and APLP2 knockout mice brains to further define their role in metal homeostasis. These studies add to the growing body of data that APP-family are metalloproteins which have shared as well as distinct effects on metals. As we continue to delineate the cellular effects of the APP-family it is important to consider how metals are involved in their actions.

## Introduction

The amyloid precursor protein (APP) is a type I transmembrane glycoprotein and a member of the multigene family that contains the paralogues amyloid precursor-like protein 1 and 2 (APLP1 and APLP2).<sup>1</sup> The metabolism of APP has been intensely studied due to it being the source of the neurotoxic amyloid beta (A $\beta$ ) peptide which is central to Alzheimer's Disease (AD) pathogenesis. Unlike APP, neither APLP1 nor APLP2 contain the A $\beta$  peptide sequence, but all three paralogues are similarly processed by the same  $\alpha$ -,  $\beta$ - and  $\gamma$ -secretases (reviewed by Walsh *et al* and Muller *et al*).<sup>2,3</sup> APP and APLP2 are expressed ubiquitously throughout the body and highest concentrations are in the central nervous system predominantly co-expressed in the same neuronal populations.<sup>1,4</sup> Although the phenotypes of single knockout (-/-) mice are fairly mild, *in vivo* and *in vitro* studies suggest that the APP gene family of proteins functions include cell and synaptic adhesion, promote synaptotrophic and neuroprotective activity and have roles in the intracellular signalling and

regulation of gene expression (reviewed by Walsh *et al* and Muller *et al*).<sup>2,3</sup> While the single gene knockout and the combined double APP<sup>-/-</sup>APLP1<sup>-/-</sup> mice produce viable offspring, when deleting APLP2 in combination with either APP or APLP1 (APP<sup>-/-</sup>APLP2<sup>-/-</sup> or APLP1<sup>-/-</sup>APLP2<sup>-/-</sup>) causes embryonic lethality suggesting that the APLP2 protein has a key physiological role for animal survival.<sup>5,6</sup> The APP gene family are classified as metalloproteins because they play an essential role in regulating cellular metal homeostasis which has both physiological as well as pathological consequences.<sup>7-9</sup>

APP has a copper-binding domain (CuBD) located in the N-terminal cysteine-rich region<sup>10,11</sup> and the full-length protein, as well as peptides derived from the CuBD, are able to coordinate and reduce Cu<sup>2+</sup> to Cu<sup>+</sup>.<sup>11-13</sup> The tertiary structure of the APP CuBD is an  $\alpha$ -helix packed over a triple strand  $\beta$ -sheet topology.<sup>14</sup> This characteristic secondary structure is shared by three other proteins known to be involved in copper chaperone activity - the Menkes copper-transporting ATPase fragment,<sup>15</sup> the metallochaperone Atx1<sup>16</sup> and the SOD1 copper chaperone.<sup>17</sup> *In vivo*, brain Cu levels display an age dependent increase over time<sup>9</sup> while the APP<sup>-/-</sup> and APLP2<sup>-/-</sup> adult mice have significantly elevated copper levels in the cerebral cortex compared to wt.<sup>9,13</sup> Conversely, in transgenic mice that overexpress APP have reduced Cu levels in the brain.<sup>18-20</sup> *In vitro* cell culture models using primary cortical neurons or embryonic fibroblasts derived from the APP-family of knockout mice demonstrated that they had accumulated

<sup>a</sup> Department of Pathology and Bio21 Molecular Science and Biotechnology Institute, The University of Melbourne, Victoria 3010, Australia.

<sup>b</sup> Australian Synchrotron, Victoria 3168, Australia.

<sup>c</sup> CSIRO Materials Science and Engineering, Victoria 3189, Australia.

<sup>d</sup> Elettra Sincrotrone Trieste S.C.p.A. S.S. 14, 34149 Trieste-Basovizza, Italy.

<sup>e</sup> X-ray Science Division Advanced Photon Source, Argonne National Laboratory, Argonne, IL 60439, USA.

<sup>f</sup> The Florey Institute of Neuroscience and Mental Health, The University of Melbourne, Victoria 3010, Australia.

\* E-mail: j.ciccotosto@unimelb.edu.au

1 exogenously added Cu indicating that APP and APLP2 have an  
2 important role in regulating copper homeostasis in these cells.<sup>8</sup>

3 Aberrant metal homeostasis is observed in patients with AD  
4 and this may contribute to AD pathogenesis, by enhancing the  
5 formation of reactive oxygen species (ROS) and toxic A $\beta$   
6 oligomers, and facilitating the formation of the hallmark  
7 amyloid deposits in AD brain.<sup>21</sup> Abnormal metabolism of APP  
8 and A $\beta$  would impair brain metal homeostasis, as part of the  
9 AD pathogenic process. A $\beta$  and APP expression can decrease  
10 brain Cu levels, whereas increasing brain Cu availability results  
11 in decreased levels of A $\beta$  and amyloid plaque formation in  
12 transgenic mice.<sup>22-24</sup> Lowering Cu levels can down-regulate the  
13 transcription of APP, strengthening the hypothesis that APP  
14 and A $\beta$  form part of the Cu homeostatic machinery in the brain.  
15 However, an unresolved question is the cellular location of the  
16 metals in individual brain neurons from APP $^{-/-}$  and APLP2 $^{-/-}$   
17 mice compared to wt. This study provides useful insights into  
18 how the APP gene family modulates metal homeostasis, as well  
19 as the function of the APP-family. This study used the X-ray  
20 fluorescence microscopy (XFM) instrumentation based at the  
21 Advanced Photon Source (APS, Argonne, IL) and from the  
22 XFM beamline at Australian Synchrotron to both localize and  
23 measure metals in primary cortical neurons and brain tissue  
24 slices from mice of the APP family of gene knockouts.

## 27 Methods

### 28 Materials

29 Unless otherwise stated all reagents were analytical grade or  
30 higher and purchased from Sigma-Aldrich (St Louis, MO).  
31 Milli-Q ultraclean water (18.2 M $\Omega$ .cm resistivity) was used  
32 throughout this study.

### 33 Generation of APP $^{+/-}$ -APLP2 $^{-/-}$ mice

34 Generation of APP $^{-/-}$  mice<sup>25</sup> and the APLP2 $^{-/-}$  mice<sup>26</sup> has  
35 previously been described. The wild type mice  
36 (APP $^{+/+}$ -APLP2 $^{+/+}$ ), APP $^{-/-}$ , APLP2 $^{-/-}$ , and APP $^{+/-}$ -APLP2 $^{-/-}$   
37 knockout mice were of the same C57BL6J x 129/Sv  
38 background strain (n=5, 6, 6, and 6 respectively). Genotypes  
39 were determined by PCR using specific primer sets.<sup>26</sup> Animals  
40 were housed with a 12 hr light/dark cycle, the room  
41 temperature set at 21 $^{\circ}$ C, the humidity which is measured  
42 coming out of the individually ventilated cages, ranges from 40  
43 to 65%. These mice also had ad libitum access to standard  
44 rodent chow and filtered (0.2 micron) tap water for drinking.

### 45 Primary neuronal cultures

46 Mouse cortical neuronal cultures were prepared under sterile  
47 conditions as described previously and approved by a local  
48 institutional Ethics committee.<sup>27,28</sup> Briefly, embryonic day 14  
49 BL6Jx129sv mouse cortices were removed, dissected free of  
50 meninges, and dissociated in 0.025% (w/v) trypsin in Krebs  
51 buffer. The dissociated cells were triturated using a filter-  
52 plugged fine pipette tip, pelleted, resuspended in plating  
53 medium (minimum Eagle's medium, 10% fetal calf serum, 5%  
54 horse serum), and counted. Poly-D-lysine coated silicon nitride

windows (area 2 x 2 mm, 5 x 5 mm frame, thickness 1,000nm)  
manufactured by Silson (Blisworth, UK) were placed in 4 well  
plates and cortical neurons seeded at a density of 75,000  
cells/well in plating medium. All cultures were maintained in an  
incubator (lined with stainless steel) set at 37  $^{\circ}$ C with 5% CO $_2$ .  
After 2 h the plating medium was replaced with fresh  
neurobasal medium containing B27 supplements, geneticin, and  
0.5 mM glutamine (all tissue culture reagents were purchased  
from Invitrogen unless otherwise stated). This method resulted  
in cultures highly enriched for neurons (>95% purity) with  
minimal astrocyte and microglial contamination as determined  
by immunostaining of culture preparations using specific  
marker antibodies (data not shown).

After 5 days in culture, neurons were washed with  
phosphate-buffered saline (PBS) pH 7.2, followed by fixation  
in 4% paraformaldehyde in PBS for 20 min. Neurons were  
washed again in PBS then residual PBS was removed by  
washing in isotonic 0.1M ammonium acetate and then allowed  
to air dry for several days before imaging.

Optical images of the cells were captured on a DMXRE  
microscope (Leica Microsystems, Wetzlar, Germany) by using  
Normaski differential interference contrast microscopy and x40  
and x100 air objectives with a Sensicam QE camera (Cooke  
Co., Auburn Hills, MI) and processed with SLidebook software  
(intelligent Imaging Innovations, Denver, CO).

### 49 Preparation of Brain slices for imaging

50 Brains were harvested from 1 and 6 month old wt, APP $^{-/-}$ , and  
51 APLP2 $^{-/-}$  mice (N=3 per group) that were transcardially  
52 perfused while under anesthesia with a high-purity solution of  
53 4% paraformaldehyde in PBS. These procedures were approved  
54 by local institutional Ethics Committee. The brains were  
55 removed then put into a sucrose solution overnight at 4  $^{\circ}$ C  
56 before snap freezing in liquid nitrogen cooled isopentane and  
57 stored at -80  $^{\circ}$ C before sectioning. Brains were warmed to -20  
58  $^{\circ}$ C and a cryostat used to cut serial slices of 12 micron  
59 thickness from each of the brains before adhering to the silicon  
60 nitride windows (2 micron thick; 5 x 5 mm<sup>2</sup> window within a  
10 x 10 mm<sup>2</sup> silicon frame). The brain slices were allowed to  
air dry overnight before further analysis.<sup>29</sup>

### 61 X-ray fluorescence Microscopy

62 For the data acquisition of the primary cultured neurons,  
63 imaging data was acquired using the scanning X-ray  
64 microprobe at beamline 2-ID-D and 2-ID-E at the Advanced  
65 Photon Source (APS, Argonne, IL) and from the XFM  
66 beamline at Australian Synchrotron. For the data collected at  
67 APS, incident X-rays of 10 keV energy were chosen to excite  
68 elements from P to Zn. A Fresnel zone plate optics (X-radia,  
69 Concord, CA) was used to focus the X-ray beam to a spot size  
70 of 0.1 x 0.1  $\mu$ m<sup>2</sup> on the specimen. Cells were raster-scanned in  
steps of 0.4  $\mu$ m per pixel, and fluorescence spectra were  
collected for 1 sec per pixel dwell time using a three-element  
UltraLE GE-detector (Canberra, Meriden, CT). Typically a 25  
by 25  $\mu$ m area were typically scanned. For "zoomed" images,  
cells were raster-scanned in steps of 0.1  $\mu$ m per pixel, and

fluorescence spectra were collected for 1 sec per pixel dwell time and 5 by 5  $\mu\text{m}$  area were typically scanned for analysis. This approach provided greater contrast in the resulting elemental maps for regions of special interest. For data collected at the Australian Synchrotron, neurons were scanned using a zone-plate nanoprobe (X-radia, Concord, CA) equipped with a single element Vortex-EM energy-dispersive detector.<sup>30</sup> As above the 10-keV excitation beam was chosen to excite elemental fluorescence from elements with an atomic number < 30. The X-ray focus was around 0.4  $\mu\text{m}$  in diameter, and so cells were raster-scanned in 0.4  $\mu\text{m}$  steps, with fluorescence spectra collected for 1 sec per pixel dwell.

Metal distributions in the mouse brain sections were mapped using a monochromatic 12.73 keV X-ray beam focused to a FWHM spot size of around 2 microns using the Kirkpatrick-Baez mirror pair. The sample stage was fly scanned (0.128 mm/s) over a selected region on window area with a step size of of 2 x 2 micron (15.6 ms dwell per 2  $\mu\text{m}$  pixel). Full-spectral images were obtained using the Maia detector and quantitation was performed using GeoPIXE software and by measurement of foils of calibrated area density.<sup>31</sup>

### Quantitation and image-processing

For the primary cell cultures, the quantitation and image-processing of all nanoprobe data were performed using MAPS software<sup>32</sup> and standardization to convert the fluorescence signal to a two-dimensional concentration in  $\mu\text{g}/\text{cm}^2$  was achieved by fitting spectra against the signal derived from thin-film standards NBS-1832 and NBS-1833 (National Bureau of Standards, Gaithersburg, MD). The integrated spectra was generated using the MAPS software and used to calibrate the metal concentrations in each sample analysed (Fig 1A). The region of interest (ROI) of each cell was determined by tracing around individual cells manually using the MAPS software and the metal content of the highlighted region used for subsequent analysis (Fig 1B). For the brain slices, the calibrated images using GeoPIXE software were saved in a tif file format. These files were imported into ImageJ software (1.48s) and the average pixel intensity determined for each image slice. The data set were normalized to the average pixel intensity of the wt brain slices.

### Statistical analysis.

When comparing the mean of two groups this study made use of Student's *t*-test, with Welch's correction, to account for unequal variances. When indicated one way analysis of variance (*anova*) was used to interrogate differences within three or more groups and a post-hoc Tukey test was used to identify differences between group means. Throughout this work the significance level is defined as \*, #;  $p < 0.05$ , \*\*, ##;  $p < 0.01$ , \*\*\*, ###;  $p < 0.001$ . The statistical tests and graphing of data were done using the Graphpad Prism v6 software. Results were presented as the mean  $\pm$  sem.

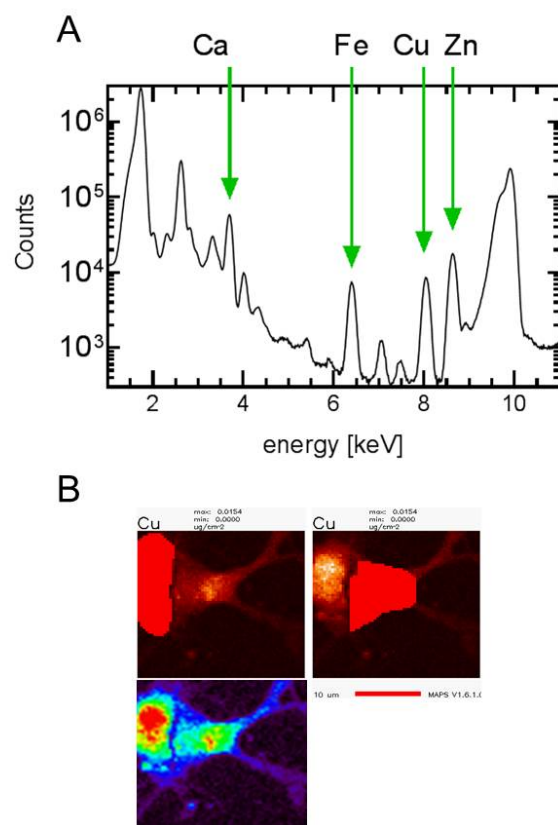


**Fig 1.** Integrated Spectra and ROI analysis of cells. **A.** This representative integrated spectra was generated using the MAPS software and used to calibrate the metal concentrations in each sample analysed. **B.** The ROI of each cell was determined by tracing around each cell manually using the MAPS software and the metal content of the highlighted region used for subsequent analysis.

## Results

### Neuronal size, phosphorus and sulphur content were decreased in mice lacking APLP2.

The bioinorganic metabolism of primary cortical neurons from wt, APP<sup>-/-</sup>, APLP2<sup>-/-</sup> and APP<sup>+/-</sup>APLP2<sup>-/-</sup> mice were investigated by measuring the concentration of various elements in individual neurons derived from the cortex of embryonic day 14 (E14) mice. The concentration and distribution of the different elements were determined at each pixel location and the resultant calibrated data used to generate elemental maps. The neuronal cell body was manually selected and included only the cell body without extended cell processes (Fig 1 B). The total number of pixels analysed per cell body area were similar for wt (673  $\pm$  60 pixels) and APP<sup>-/-</sup> (769  $\pm$  92) and significantly higher in the APLP2<sup>-/-</sup> (1662  $\pm$  215 pixels,  $p < 0.01$ ) and APP<sup>+/-</sup>APLP2<sup>-/-</sup> (1381  $\pm$  141 pixels,  $p < 0.05$ ) compared to wt. As expected, the calculated area for the neuronal cell body for wt and APP<sup>-/-</sup> genotype were similar while neurons lacking APLP2 protein (APLP2<sup>-/-</sup> and APP<sup>+/-</sup>

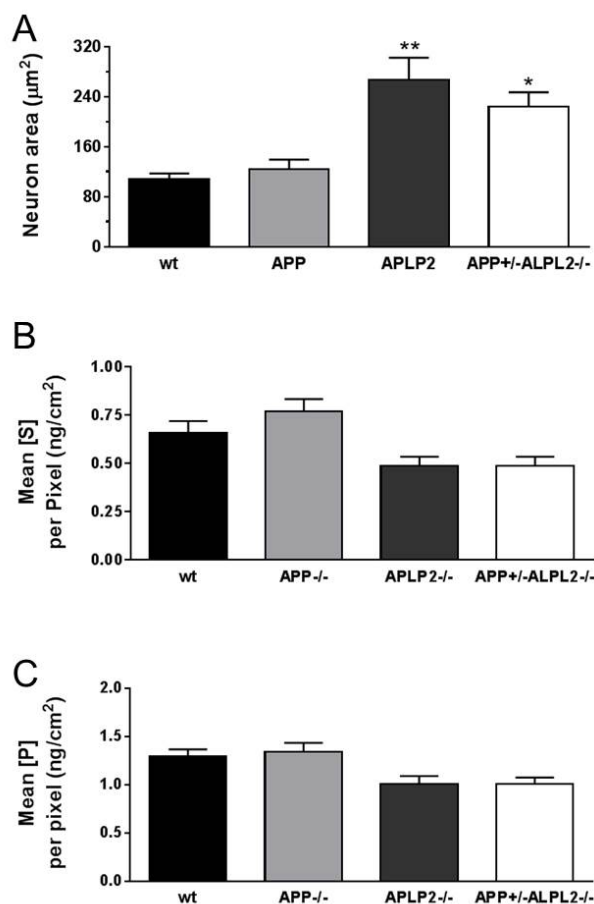


**Fig 2.** Neuronal area and endogenous S and P levels. The (A) ROI area was calculated and the (B) S and (C) P concentration per pixel was determined in neurons from the wt, APP<sup>-/-</sup>, APLP2<sup>-/-</sup> and APP<sup>+/-</sup>APLP2<sup>-/-</sup> type mice. Results are mean  $\pm$  sem, n = 5-6. \*, p < 0.05; \*\*, p < 0.01 vs wt. Scale bar = 5 microns.

APLP2<sup>-/-</sup>) showed at least a two-fold increase in area size compared to the wt (Fig 2A). The presence of sulphur (S) containing amino acids (Met and Cys) occur within larger proteins with very high frequency.<sup>33,34</sup> Phosphorous (P) is a component of DNA, RNA, and ATP which are mostly concentrated within the nucleus and biological membranes. Therefore to assess whether there were differences in metabolism between the APP family genotypes, the abundance and distribution of P and S were compared. We found no significant difference in the levels of S and P or in the ratio of S/P between mice genotype groups (Fig 2B-2D) suggesting the cellular protein content is similar between all 4 genotypes examined.

#### Cu and Zn concentration distribution maps in neuronal cells

The Cu concentration distribution maps in neuronal cells from wt mice was examined by XFM and the per pixel elemental concentration presented on a linear color scale (highest = red > yellow > green > blue > purple > black = lowest). The highest areal density of Cu was observed in the cytoplasmic region of

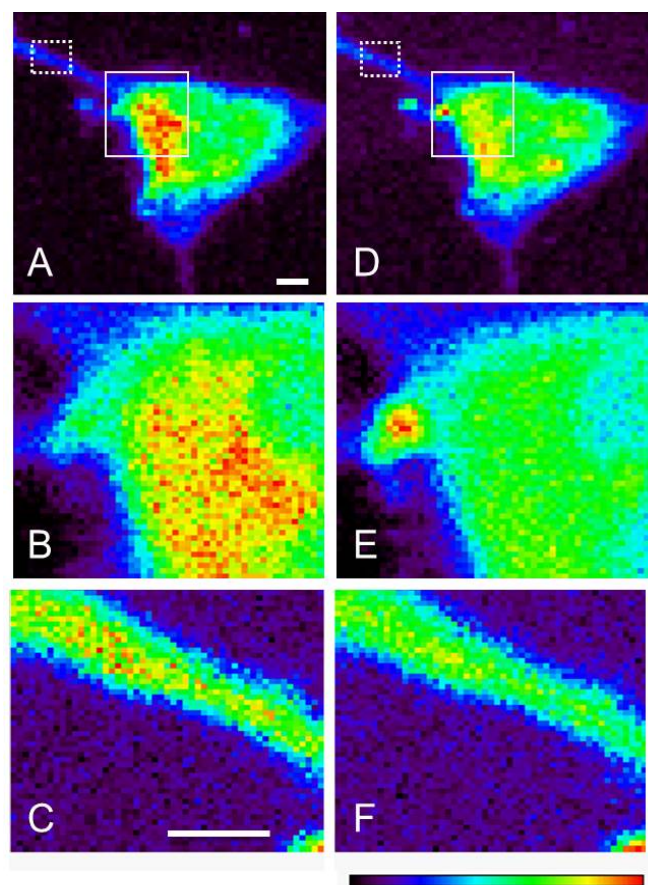


**Fig 3.** Cu and Zn concentration intensity distribution maps in single neurons from control mice. Endogenous (A) Cu and (D) Zn distribution in neurons with higher resolution area maps for cell body and portion of the axon for Cu (B and C respectively) and Zn (E and F). Scale bar = 2 microns.

the neuron and predominantly localized towards the major axon branching point (Fig 3A). Higher contrast imaging of selected regions in cells where Cu concentrations were high (Fig 3B), a portion of the axon from these same cells is shown in Fig 3C, revealed an unremarkable distribution pattern. The Zn concentration distribution maps was similar to that of Cu, with the highest Zn levels present near the axon branching point (Fig 3D). Higher definition of the cell body and axon terminal illustrate Zn levels are more evenly spread throughout these regions compared to Cu (Fig 3E and 3F). In addition, the regions with higher concentrations of transition metals overlapped with elevated S (data not shown) consistent with expectations that there will be little solvated Cu or Zn present within the cellular milieu. Further, the ratio of S/Cu in the wt neurons was around .07 and at least 10 fold lower compared to what has been reported in astrocytes<sup>35</sup> suggesting that the metals would be bound to large cellular proteins such as SOD1.

#### Distribution of Cu and Zn shows substantial overlap in neurons in all four genotypes.

To test the degree of co-localization between Cu and Zn, the Cu and Zn maps were overlaid and the Cu/Zn ratio calculated for

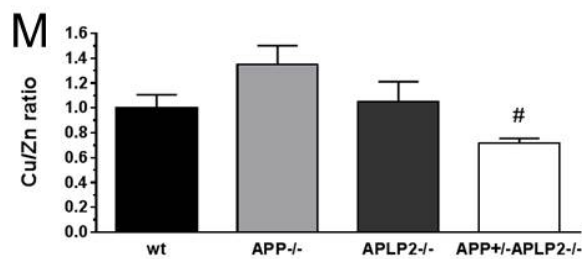
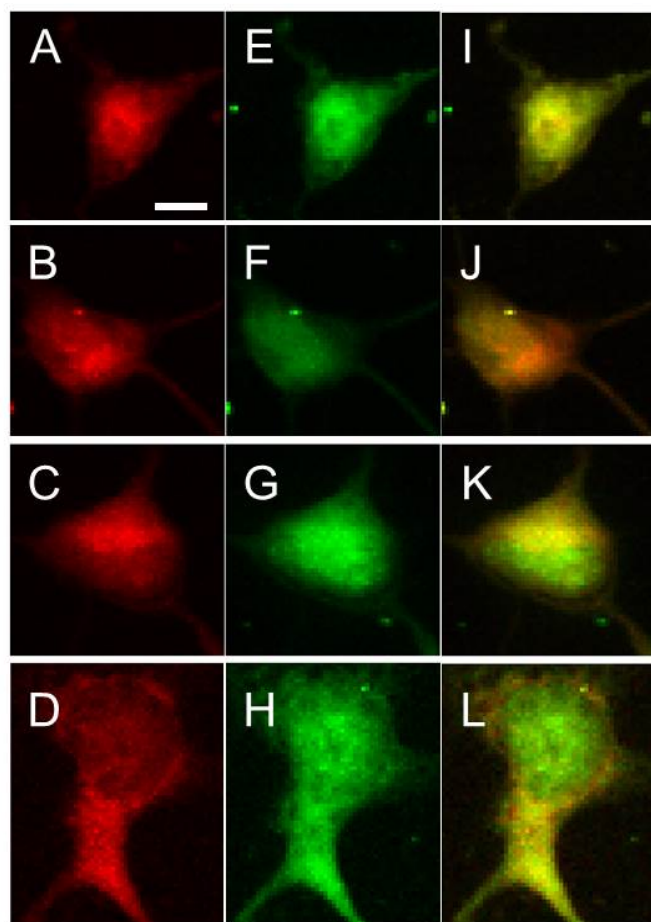


**Fig 4.** Cu and Zn colocalization images in the different mouse knockout genotypes. (A-D) Cu levels in neurons are represented by the red color and (E-H) Zn levels in neurons are shown in green color while the combined (I-L) Cu and Zn images show overlapping areas in yellow color. Primary cortical neurons from wt (A, E, I); APP<sup>-/-</sup> (B, F, J); APLP2<sup>-/-</sup> (C, G, K); APP<sup>+/-</sup>APLP2<sup>-/-</sup> (D, H, L) mice were compared and the Cu/Zn ratio for each genotype plotted (M). Results are mean ± sem, n=5-6, #, p<0.05 vs APP<sup>-/-</sup>. Scale bar = 5 microns.

all 4 genotypes (Fig 4). The overlay of the Cu (green) and Zn (red) resulted in mostly yellow and green coloured areas in the cells for wt, APLP2<sup>-/-</sup> and the neurons. The APP<sup>-/-</sup> neurons were predominantly orange coloured suggesting that there was more Cu than Zn and this was confirmed by calculating a higher Cu/Zn ratio compared to the other 3 genotypes (Fig 4M). In contrast, the APP<sup>+/-</sup>APLP2<sup>-/-</sup> neuron had lower Cu/Zn ratio compared to the other genotypes and was significantly lower

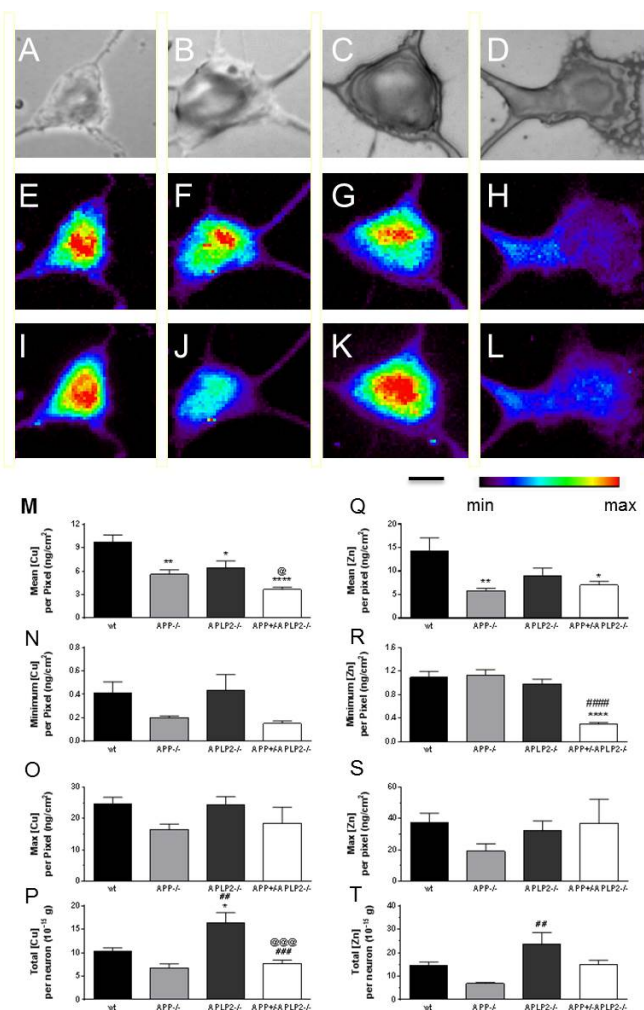


**Fig 5.** Cu and Zn distribution maps and concentrations in primary cortical neurons from different mice genotypes. Phase images were taken from neurons isolated from (A) wt, (B) APP<sup>-/-</sup>, (C) APLP2<sup>-/-</sup> and (D) APP<sup>+/-</sup>APLP2<sup>-/-</sup> genotypes examined. The metal distribution maps for Cu (E-H) and Zn (I-L) were prepared for the different genotypes respectively with the minimum and maximum (Min - Max) intensity rainbow map settings for Cu (0.6-20 ng/cm<sup>2</sup>) and Zn (0.6-35 ng/cm<sup>2</sup>) were identical across the different mice genotypes examined. The quantitated Mean, Minimum, Maximum and Total metal concentrations for Cu (M-P respectively) and Zn (Q-T respectively) were determined for the different mice genotypes. Results are mean ± sem, n=5-6. \*, p<0.05; \*\*, p<0.01, \*\*\*, p<0.001; \*\*\*\*, p<0.0001 vs wt, # vs APP<sup>-/-</sup>, and @ vs APLP2<sup>-/-</sup>. Scale bar = 5 microns.

compared to APP<sup>-/-</sup> neuron only. Overall, the data highlights that the majority of the cellular Cu and Zn are co-located and this suggests that they are likely bound to metalloproteins such as the Cu/Zn SOD-1 protein 36 or metallothionein 35. Neurons derived from all 4 genotypes showed some degree of co-registration indicating that Cu and Zn metabolism are not completely orthogonalized by the loss of APP or its paralogues.

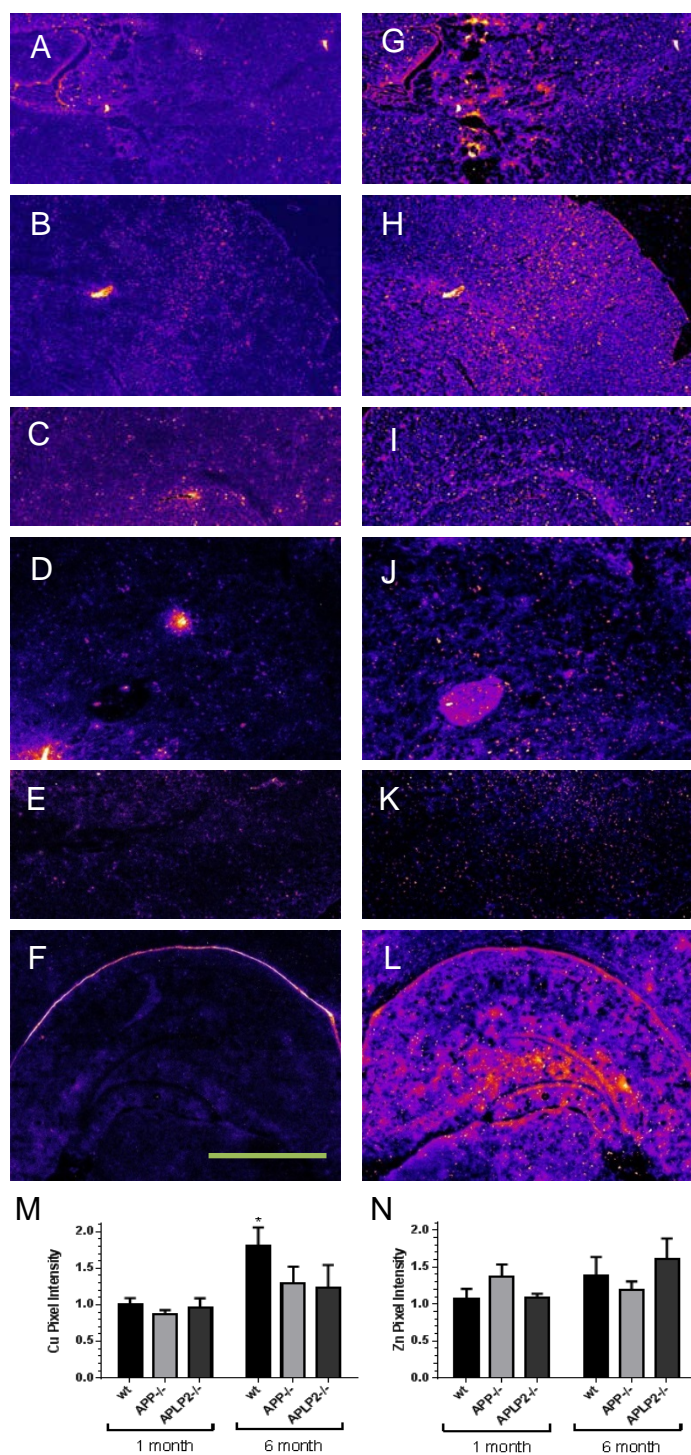


**Fig 6.** Cu and Zn distribution maps and pixel intensity quantitation in 1 and 6 month old adult brain slices from different mice genotypes. Metal distribution maps for Cu (A -F) and Zn (G-H) were prepared from 1 month (A-C, G-I) and 6 month (D-F, J-L) old adult mice brains from wt (A, G, D, J), APP<sup>-/-</sup> (B, H, E, K), and APLP2<sup>-/-</sup> (C, I, F, L). The Cu (M) and Zn (N) pixel intensity levels were quantitated for the adult brain slices and the data normalized to the 1 month old wt brain slices. Results are mean  $\pm$  sem,  $n=3$ . \*,  $p<0.05$ ; vs 1 month old wt. Scale bar = 1 mm.

### Concentrations for Cu and Zn are altered in primary cortical neurons lacking APP and APLP2.

The metal concentrations of Cu and Zn were determined in individual neuronal cells from the 4 mouse genotype variants (Fig 5). The mean Cu concentration per pixel was significantly lower in neurons for both the APP<sup>-/-</sup> and APLP2<sup>-/-</sup> (41% and 33% respectively) compared to the wt (Fig 5M). For the double APP<sup>+/-</sup>-APLP2<sup>-/-</sup> genotype neurons, the mean Cu concentration per pixel was significantly lower compared to both APLP2<sup>-/-</sup> and wt (29% and 62% respectively, Fig 5M). To determine whether there was any variance in the concentration of the metals throughout the neuron, we compared the minimum (min) and maximum (max) metal concentrations per pixel. The min Cu (Fig 5N) and max Cu (Fig 5O) concentration per pixel were similar between the 4 genotypes examined suggesting that the Cu distribution throughout the neuron cell body is fairly uniform considering at least 600 data points (or pixels) were examined in the wt neurons alone. The total element concentration per neuron, which represents the sum total of each pixel Cu concentration inside each cell body area, was significantly elevated in the APLP2<sup>-/-</sup> neuron compared to wt and APP<sup>-/-</sup> and the double APP<sup>+/-</sup>-APLP2<sup>-/-</sup> neuron (Fig 5P). The concentration of Zn, like Cu, was significantly lower in the APP<sup>-/-</sup> and APP<sup>+/-</sup>-APLP2<sup>-/-</sup> knockout neurons by 59% and 51% respectively compared to the wt neurons while the APLP2<sup>-/-</sup> levels were decreased by 37% and not statistically different (Fig 5Q). While the minimum Zn concentration per pixel for the APP<sup>+/-</sup>-APLP2<sup>-/-</sup> mice were significantly lower compared to wt and APP<sup>-/-</sup> neurons (Fig 5R), the minimum levels between the wt and single knockout neurons were similar and the max Zn concentrations per pixel between the 4 genotypes were similar too (Fig 5S). The total Zn concentration per neuron was significantly higher only in APLP2<sup>-/-</sup> compared to APP<sup>-/-</sup> neurons (Fig 5T).

### Localization of transition metals in mouse brain slices.

Having established that metal levels are significantly altered in single cultured neurons from embryonic mice, we then examined metal distribution in brain slices from 1 month (Fig 6A-C, G-I) and 6 month old adult mice (Fig 6D-F, J-L). We compared the metal distribution patterns on a gross scale examining the hippocampal and cortical regions in the wt mice brains compared to the single knockout mice brain tissue slices only. Unlike the analysis of neurons at the single cell level, we did not observe any differences in the distribution patterns for Cu (Fig 6A-F) and Zn (Fig 6G-L) throughout the tissue slices between the different genotypes and between the two different age groups at the gross anatomical level. Further analysis of the brain slices were performed and the average pixel intensity levels were measured in the brain slices for Cu and Zn (Fig 6M and 6N respectively) and scanned intensity levels normalized to the 1 month old wt brain tissue slice. This analysis showed that the Cu concentrations were lower for the APP and APLP2 KO brains slices compared to wt but this was not found to be statistically different. However we did find that the Cu levels

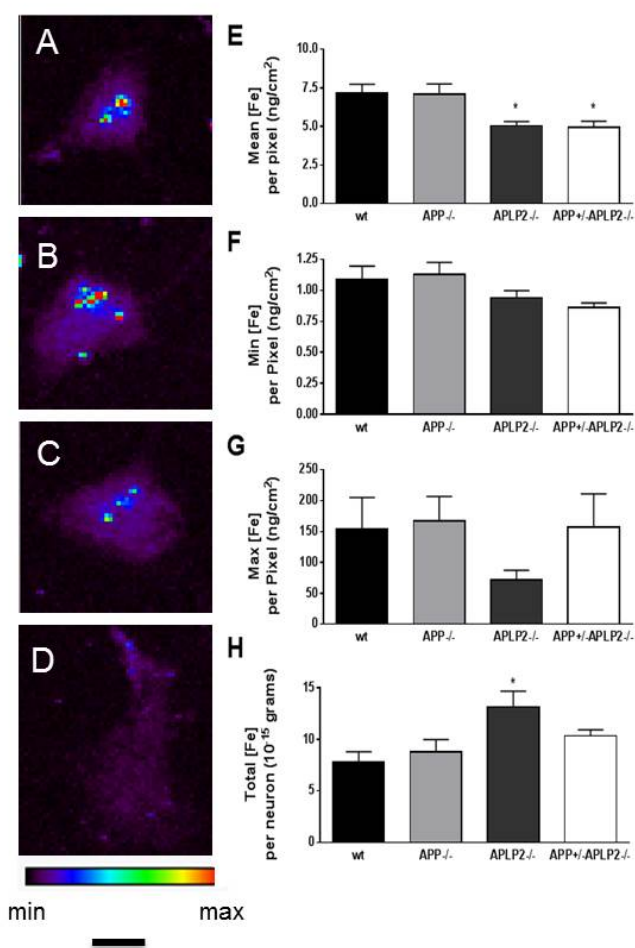


**Fig 7.** Fe distribution maps and concentrations in primary cortical neurons from different mice genotypes. Metal distribution maps from neurons isolated from (A) wt, (B) APP<sup>-/-</sup>, (C) APLP2<sup>-/-</sup> and (D) APP<sup>+/-</sup>APLP2<sup>-/-</sup> genotypes were examined and the minimum and maximum (Min - Max) intensity settings for Fe (0.6 – 90 ng/cm<sup>2</sup>) were identical across the different mice genotypes examined. The Fe levels were quantitated and the (E) Mean, (F) Minimum, (G) Maximum and (H) Total metal concentrations were calculated for the different mice genotypes examined. Results are mean +/- sem, n= 5-6. \*, p<0.05; vs wt. Scale bar = 5 microns.

were significantly higher at 6 months of age compared to 1 month for wt only (Fig 6M). Zn levels across the 3 genotypes and two age groups were relatively unchanged (Fig 6N).

#### Concentrations for Fe are altered in primary cortical neurons lacking APP and APLP2.

The distribution of Fe in neurons differs considerably to Cu and Zn where it is found to be much more concentrated and limited to only a few pixels in all genotypes examined (Fig 7). The mean Fe concentration per pixel was significantly lower in APLP2<sup>-/-</sup> and APP<sup>+/-</sup>APLP2<sup>-/-</sup> neurons only (Fig 7E). While the min and max Fe concentration per pixel were not statistically different between the 4 mouse genotypes examined, there is a greater than 150-fold difference in the concentration of Fe between the lowest and highest Fe concentrations (Fig

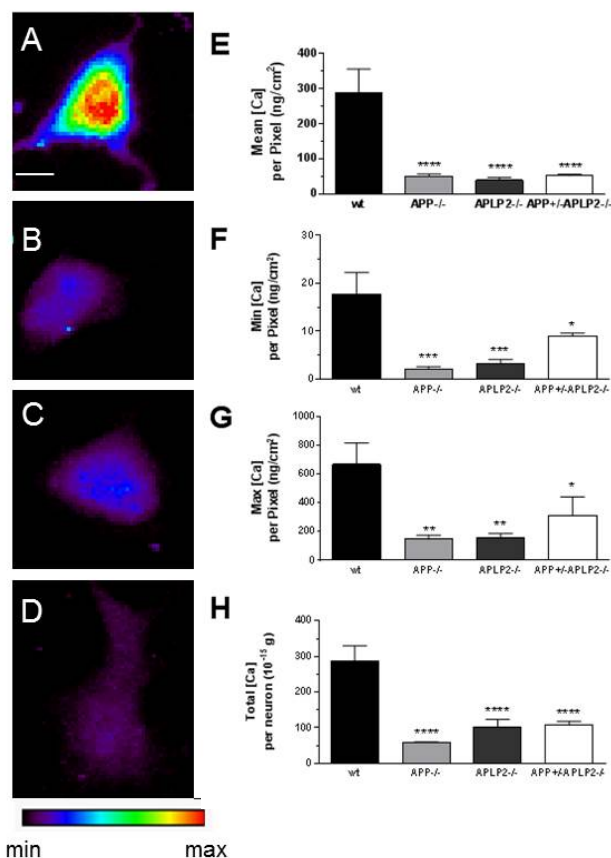


**Fig 8.** Ca distribution maps and concentrations in primary cortical neurons from different mice genotypes. Metal distribution maps from neurons isolated from (A) wt, (B) APP<sup>-/-</sup>, (C) APLP2<sup>-/-</sup> and (D) APP<sup>+/-</sup>APLP2<sup>-/-</sup> genotypes were examined and the minimum and maximum (Min - Max) intensity settings for Ca (2 – 700 ng/cm<sup>2</sup>) were identical across the different mice genotypes examined. The (E) Mean, (F) Minimum, (G) Maximum and (H) Total metal concentrations were calculated for the different mice genotypes examined. Results are mean +/- sem, n=5-6. \*, p<0.05; vs WT. Scale bar = 5 microns.

7F-G) compared to a 60 to 70-fold difference was calculated for the Cu and Zn elements (Fig 5). Total Fe concentration per neuron was significantly higher in the APLP2<sup>-/-</sup> neuron compared to the wt neuron.

#### Concentrations for Ca are dramatically decreased in primary cortical neurons lacking APP and APLP2 expression.

The mean Ca concentration per pixel in the single APP<sup>-/-</sup> and APLP2<sup>-/-</sup> and double knockout APP<sup>+/-</sup>APLP2<sup>-/-</sup> neurons were significantly lower compared to the wt neurons (Fig 8E). In fact, even the min and max and total Ca concentration per pixel were significantly lower in the neurons from the knockout mice compared to the wt (Fig 8F, G, H respectively). However, the Ca concentrations between the knockout mice genotypes were similar for each analysis group. In addition, the knockout neurons contain on average, around 80% less Ca compared to the wt neurons across all parameters examined.

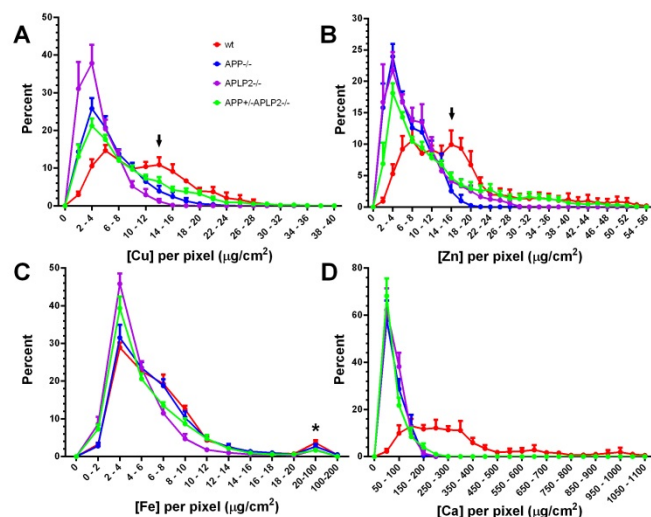


**Fig 9.** Analysis of the selected metal concentration per pixel in primary cortical neurons from different mice genotypes. For comparison between genotypes, the metal concentration per pixel for each neuronal cell body area was examined by binning the data set and plotting the normalized frequency distribution for each metal (A) Cu, (B) Zn, and (C) Fe. Results are mean  $\pm$  sem,  $n=5-6$ .

### The frequency distribution for the Cu, Zn and Ca concentration per pixel within the cell body area was altered in neurons lacking APP or APLP2 expression.

To get a better understanding of the metal homeostasis within a cell, the XFS technique will measure metal concentrations at a resolution of  $0.1 \mu\text{m}^2$  per pixel therefore generating from 600 to 1600 data points per neuron for analysis. The metal concentration of each pixel were binned into narrow concentration ranges ( $0.002 \mu\text{g}/\text{cm}^2$  for Cu, Zn, and Fe and  $0.05$  for Ca) and the frequency distribution data set was normalized to the total number of pixels analysed per cell. Using this procedure, we observed a striking difference in the distribution patterns for the Cu, Zn, and Ca elements when comparing between the wt mice to mice lacking APP or APLP2 (Fig 9). In wt neurons, Cu and Zn displayed a bimodal distribution pattern; a lower concentration range of peaking at 4-6 and 6-8  $\mu\text{g}/\text{cm}^2$  and at 2- to 3-fold higher range of 12-14 and 14-16  $\mu\text{g}/\text{cm}^2$  respectively. While in neurons lacking APP or APLP2, the peak at the higher concentration range (as denoted by the arrow in Fig 9A and 9B) is no longer evident, rather a single peak was observed at a lower concentration of 2-4  $\mu\text{g}/\text{cm}^2$  for both metals. The concentration and distribution pattern for Fe was similar across the four mice genotypes with the majority of the Fe concentration distribution pattern ranging between 2 - 4  $\mu\text{g}/\text{cm}^2$ . The concentration of Fe in the few pixels colored red on the elemental distribution MAPS (Fig 7) were at least 10- to 50-fold higher in concentration (see \* in Figure 9C). Unlike Cu and Zn which had a clear bimodal distribution pattern, the distribution frequency for the Ca metal concentration was simply uniform across a broad range (100 to 350  $\mu\text{g}/\text{cm}^2$ ) in the

wt neurons while in the cells lacking APP or APLP2, a single narrow peak with a concentration range of 0 to 5  $\mu\text{g}/\text{cm}^2$  was observed (Fig 9D).

## Discussion

APP and APLP2 are important modulators of brain metal homeostasis since altering APP and APLP2 expression levels is associated with significant changes in Cu, Zn and Fe homeostasis.<sup>7-9,13,24,37</sup> While previous studies examined metal levels in whole brains or in whole cell culture models using inductively coupled plasma mass spectrometry (ICP-MS) or atomic absorption spectrometry, this current study used XFM to both localize and quantitate metals levels in response to changes in APP-family expression. The advantage of using XFM is that it provides high elemental sensitivity for investigating medium to high trace metal elements, irrespective of its coordination or redox status, and provide a higher level of resolution and thereby enabling greater quantitative information and spatial mapping of metal elements in biological structures at the submicron scale. Analysis of the elemental maps and examination of the frequency distribution of the metal concentrations, we observed a dramatic shift in the manner in which neurons can store the metal elements. Not only were the concentration of the Cu, Zn, and Fe significantly altered in neurons lacking APP and or APLP2 expression, now we can also include Ca to this list of metals that is significantly altered. Therefore, using this technology, we were able to extend our understanding of how APP and APLP2 protein expression affects metal homeostasis and cellular distribution in neurons at the single cell level.

Under basal culture conditions, endogenous APP normally resides in a perinuclear location in the neuron<sup>38</sup> and it will redistribute to the plasma or Golgi compartment depending on whether the Cu concentration in the conditioned media is removed by chelation or elevated.<sup>39</sup> Under basal culture conditions, we observed that the highest accumulation of Cu was localized to the cytoplasmic compartment of the cell with an apparent peri-nucleus localization as illustrated by the red colored pixels shown on the elemental distribution maps (Fig 5). This Cu distribution pattern was similarly seen in different cell types such as endothelial and fibroblasts.<sup>35,40,41</sup> Although the images illustrating the Cu elemental maps for APP and APLP2 knockout neurons were similar, the cellular Cu levels were significantly altered compared to wt. Further analysis of the Cu concentrations at each pixel, we discovered that the Cu concentration appears to exist in a binomial manner in wt neurons, while in the neurons from the knock out mice, only a lower concentration peak distribution was observed suggesting that both APP and APLP2 protein expression are important for maintaining Cu homeostasis in neurons. Like the neurons in culture, Cu levels brain slices from adult mice were 10 - 20 % and 50% lower from 1 and 6 month old mice respectively but these levels were not statistically significant which is most likely due to the limited number of brains slices that were examined in this experiment. In addition, Cu levels were higher

1 in the 6 month old brains compared to the 1 month old brains  
2 for all genotypes examined confirming that brain Cu levels  
3 increase with age.<sup>9</sup>

4 In the APP gene family, Cu and Zn bind to the E2 domain  
5 and mediate the oligomerisation of APP but not APLP2.<sup>42</sup> Like  
6 Cu, the mean Zn concentration per pixel was significantly  
7 decreased in APP<sup>-/-</sup> and APLP2<sup>-/-</sup> APP<sup>+/-</sup>, but not in the  
8 APLP2<sup>-/-</sup> cells. While the total Zn concentration per neuron  
9 was still significantly lower in the APP<sup>-/-</sup> neurons, conversely,  
10 like Cu, the total Zn concentration per neuron was significantly  
11 higher in APLP2<sup>-/-</sup> neurons. The higher total Zn concentration  
12 in the embryonic APLP2<sup>-/-</sup> neurons can explain why total Zn  
13 concentration levels in whole mouse brain was significantly  
14 elevated in adult APLP2<sup>-/-</sup> mice.<sup>9</sup> Like Cu, the Zn  
15 concentration per pixel analysis showed a similar alteration  
16 from a binomial to unimodal concentration distribution in the  
17 neurons lacking APP gene family of proteins. Therefore, the  
18 higher Zn concentration measured in these neurons suggests  
19 that APLP2 also has a regulatory role in neuronal Zn  
20 homeostasis.

21 Based on our ROI analysis data, the size of the primary  
22 cortical neurons which lack APLP2 expression were  
23 significantly larger compared to the wt and APPKO neurons  
24 suggesting that APLP2 may be important for regulating  
25 neuronal morphology. These size differences do not reflect  
26 changes in viability since we (data not shown) and others<sup>5</sup> saw  
27 no significant differences in plating efficiency or viability in  
28 culture. This significant increase in neuronal size contrasts with  
29 the observation that the APLP2<sup>-/-</sup> mice (both single and  
30 double<sup>-/-</sup>) have significantly reduced body weights and  
31 diminished head widths compared to wt.<sup>6</sup> In contrast, neurons  
32 lacking APP expression have a similar size to the wt neurons  
33 suggesting that it has a redundant role in maintaining neuronal  
34 cell size.

35 APP can facilitate Fe export from cells with APP<sup>-/-</sup> neurons  
36 exposed to Fe retaining more Fe after treatment compared to wt  
37 cells.<sup>7</sup> In this study, the mean Fe concentration per pixel in  
38 neurons under basal conditions was significantly lower in  
39 APLP2<sup>-/-</sup> neurons while the total amount of Fe was  
40 significantly higher. This higher concentration could be  
41 explained by the larger cell size observed for APLP2<sup>-/-</sup>  
42 neurons. In contrast, no changes in Fe levels were observed for  
43 the APP<sup>-/-</sup> neurons compared to wt. In whole brain, Fe  
44 concentration was significantly higher in APP<sup>-/-</sup> at 12 and 18 m  
45 compared to wt while in APLP2<sup>-/-</sup> brains, Fe was significantly  
46 lower at the younger, three month time point only.<sup>9</sup> These  
47 results confirm that APP has a more important role in  
48 regulating basal Fe levels in older adult brains while APLP2  
49 may affect Fe homeostasis in embryonic neurons.

50 A novel finding of the present study is the large decrease in  
51 Ca levels in neurons from both single and APP<sup>+/-</sup>APLP2<sup>-/-</sup>  
52 mice compared to wt mice. The reduction in intracellular Ca  
53 stores could explain the poor muscle function / reduced grip  
54 strength and locomotor activity,<sup>43</sup> decreased brain synaptic  
55 activity and spatial learning activities.<sup>44,45</sup> Synaptic  
56 transmission is largely regulated by the activation of N- and L-

type Ca channels and concomitant release of pools of Ca into  
the synaptic cleft from nerve terminals and assist in the  
activation of post synaptic sites such as the neuromuscular  
junction.<sup>46</sup> Yang et al. proposed that Ca homeostasis is  
regulated by APP since they observed increased asynchronous  
release during repetitive stimulation of the neuromuscular  
junction in APP<sup>-/-</sup> mice.<sup>46</sup> This may, in part, be explained by  
Ca levels being significantly decreased in the plasma of  
embryonic APP and APLP2<sup>-/-</sup>.<sup>6</sup>

## Conclusions

We have shed new insights into effects of APP and APLP2  
expression on the subcellular localization and distribution of  
Cu, Fe, Zn, and Ca in neurons, as well as further define their  
role in metal homeostasis. These studies add to the growing  
body of data that APP-family are metalloproteins which have  
shared as well as distinct effects on metals. As we continue to  
delineate the cellular effects of the APP-family it is important  
to consider how metals are involved in their actions.

## Acknowledgements

Work was supported by funds from the Australian Research  
Council, the Australian National Health and Medical Research  
Council and from Operational Infrastructure Support Victorian  
State Government. This research used resources of the  
Advanced Photon Source, a U.S. Department of Energy (DOE)  
Office of Science User Facility operated for the DOE Office of  
Science by Argonne National Laboratory under Contract No.  
DE-AC02-06CH11357. Access was made possible through the  
financial assistance of the Australian Synchrotron Research  
Fund (proposal AS\_IA083/APS10858). We acknowledge  
travel funding provided by the International Synchrotron  
Access Program managed by the Australian Synchrotron and  
funded by the Australian Government. Part of this research  
was undertaken on the XFM beamline at the Australian  
Synchrotron, Victoria, Australia.

## References

- 1 Wasco, W., Gurubhagavatula, S., Paradis, M. D., Romano, D. M., Sisodia, S. S., Hyman, B. T., Neve, R. L. and Tanzi, R. E., Isolation and characterization of APLP2 encoding a homologue of the Alzheimer's associated amyloid beta protein precursor, *Nat Genet*, 1993, **5**, 95-100.
- 2 Walsh, D. M., Minogue, A. M., Sala Frigerio, C., Fadeeva, J. V., Wasco, W. and Selkoe, D. J., The APP family of proteins: similarities and differences, *Biochem Soc Trans*, 2007, **35**, 416-420.
- 3 Müller, U. C. and Zheng, H., Physiological Functions of APP Family Proteins, *Cold Spring Harb Perspect Med*, 2012, **2**.
- 4 Crain, B. J., Hu, W., Sze, C. I., Slunt, H. H., Koo, E. H., Price, D. L., Thinakaran, G. and Sisodia, S. S., Expression and distribution of amyloid precursor protein-like protein-2 in Alzheimer's disease and in normal brain, *Am J Pathol*, 1996, **149**, 1087-1095.
- 5 Heber, S., Herms, J., Gajic, V., Hainfellner, J., Aguzzi, A., Rulicke, T., von Kretschmar, H., von Koch, C., Sisodia, S.,

- 1 Tremml, P., Lipp, H. P., Wolfer, D. P. and Muller, U., Mice with  
2 combined gene knock-outs reveal essential and partially  
3 redundant functions of amyloid precursor protein family  
4 members, *J Neurosci*, 2000, **20**, 7951-7963.
- 5 6 Needham, B., Wlodek, M., Ciccotosto, G., Fam, B., Masters, C.,  
7 Proietto, J., Andrikopoulos, S. and Cappai, R., Identification of the  
8 Alzheimer's disease amyloid precursor protein (APP) and its  
9 homologue APLP2 as essential modulators of glucose and  
10 insulin homeostasis and growth, *J Pathol*, 2008, **215**, 155-163.
- 11 7 Duce, J. A., Tsatsanis, A., Cater, M. A., James, S. A., Robb, E.,  
12 Wikke, K., Leong, S. L., Perez, K., Johanssen, T., Greenough,  
13 M. A., Cho, H. H., Galatis, D., Moir, R. D., Masters, C. L.,  
14 McLean, C., Tanzi, R. E., Cappai, R., Barnham, K. J.,  
15 Ciccotosto, G. D., Rogers, J. T. and Bush, A. I., Iron-export  
16 ferroxidase activity of beta-amyloid precursor protein is  
17 inhibited by zinc in Alzheimer's disease, *Cell*, 2010, **142**, 857-  
18 867.
- 19 8 Bellingham, S. A., Ciccotosto, G. D., Needham, B. E., Fodero,  
20 L. R., White, A. R., Masters, C. L., Cappai, R. and Camakaris,  
21 J., Gene knockout of amyloid precursor protein and amyloid  
22 precursor-like protein-2 increases cellular copper levels in  
23 primary mouse cortical neurons and embryonic fibroblasts, *J*  
24 *Neurochem*, 2004, **91**, 423-428.
- 25 9 Needham, B. E., Ciccotosto, G. D. and Cappai, R., Combined  
26 deletions of amyloid precursor protein and amyloid precursor-  
27 like protein 2 reveal different effects on mouse brain metal  
28 homeostasis, *Metallomics*, 2014, **6**, 598-603.
- 29 10 Hesse, L., Beher, D., Masters, C. L. and Multhaup, G., The beta  
30 A4 amyloid precursor protein binding to copper, *FEBS Lett*,  
31 1994, **349**, 109-116.
- 32 11 Multhaup, G., Schlicksupp, A., Hesse, L., Beher, D., Ruppert,  
33 T., Masters, C. L. and Beyreuther, K., The amyloid precursor  
34 protein of Alzheimer's disease in the reduction of copper(II) to  
35 copper(I), *Science*, 1996, **271**, 1406-1409.
- 36 12 Ruiz, F. H., González, M., Bodini, M., Opazo, C. and Inestrosa,  
37 N. C., Cysteine 144 Is a Key Residue in the Copper Reduction  
38 by the  $\beta$ -Amyloid Precursor Protein, *J Neurochem*, 1999, **73**,  
39 1288-1292.
- 40 13 White, A. R., Reyes, R., Mercer, J. F., Camakaris, J., Zheng, H.,  
41 Bush, A. I., Multhaup, G., Beyreuther, K., Masters, C. L. and  
42 Cappai, R., Copper levels are increased in the cerebral cortex  
43 and liver of APP and APLP2 knockout mice, *Brain Res*, 1999,  
44 **842**, 439-444.
- 45 14 Barnham, K. J., McKinstry, W. J., Multhaup, G., Galatis, D.,  
46 Morton, C. J., Curtain, C. C., Williamson, N. A., White, A. R.,  
47 Hinds, M. G., Norton, R. S., Beyreuther, K., Masters, C. L.,  
48 Parker, M. W. and Cappai, R., Structure of the Alzheimer's  
49 disease amyloid precursor protein copper binding domain. A  
50 regulator of neuronal copper homeostasis, *J Biol Chem*, 2003,  
51 **278**, 17401-17407.
- 52 15 Gitschier, J., Moffat, B., Reilly, D., Wood, W. I. and Fairbrother,  
53 W. J., Solution structure of the fourth metal-binding domain  
54 from the Menkes copper-transporting ATPase, *Nat Struct Biol*,  
55 1998, **5**, 47-54.
- 56 16 Arnesano, F., Banci, L., Bertini, I., Huffman, D. L. and  
57 O'Halloran, T. V., Solution structure of the Cu(I) and apo forms  
58 of the yeast metallochaperone, Atx1, *Biochemistry*, 2001, **40**,  
59 1528-1539.
- 60 17 Lamb, A. L., Wernimont, A. K., Pufahl, R. A., Culotta, V. C.,  
O'Halloran, T. V. and Rosenzweig, A. C., Crystal structure of  
the copper chaperone for superoxide dismutase, *Nat Struct Biol*,  
1999, **6**, 724-729.
- 18 Maynard, C. J., Cappai, R., Volitakis, I., Cherny, R. A., White,  
A. R., Beyreuther, K., Masters, C. L., Bush, A. I. and Li, Q.-X.,  
Overexpression of Alzheimer's Disease Amyloid-beta Opposes  
the Age-dependent Elevations of Brain Copper and Iron, *J Biol*  
*Chem.*, 2002, **277**, 44670-44676.
- 19 Phinney, A. L., Drisaldi, B., Schmidt, S. D., Lugowski, S.,  
Coronado, V., Liang, Y., Horne, P., Yang, J., Sekoulidis, J.,  
Coomaraswamy, J., Chishti, M. A., Cox, D. W., Mathews, P. M.,  
Nixon, R. A., Carlson, G. A., St George-Hyslop, P. and  
Westaway, D., In vivo reduction of amyloid-beta by a mutant  
copper transporter, *Proc Natl Acad Sci U S A*, 2003, **100**, 14193-  
14198.
- 20 Bayer, T. A., Schafer, S., Simons, A., Kemmling, A., Kamer, T.,  
Tepest, R., Eckert, A., Schussel, K., Eikenberg, O., Sturchler-  
Pierrat, C., Abramowski, D., Staufenbiel, M. and Multhaup, G.,  
Dietary Cu stabilizes brain superoxide dismutase 1 activity and  
reduces amyloid Abeta production in APP23 transgenic mice,  
*Proc Natl Acad Sci U S A*, 2003, **100**, 14187-14192.
- 21 Kaden, D., Bush, A. I., Danzeisen, R., Bayer, T. A. and  
Multhaup, G., Disturbed copper bioavailability in Alzheimer's  
disease, *Int J Alzheimers Dis*, 2011, **2011**, 345614.
- 22 Phinney, A. L., Drisaldi, B., Schmidt, S. D., Lugowski, S.,  
Coronado, V., Liang, Y., Horne, P., Yang, J., Sekoulidis, J.,  
Coomaraswamy, J., Chishti, M. A., Cox, D. W., Mathews, P. M.,  
Nixon, R. A., Carlson, G. A., George-Hyslop, P. S. and  
Westaway, D., In vivo reduction of amyloid- $\beta$  by a mutant  
copper transporter, *Proc Natl Acad Sci U S A*, 2003, **100**, 14193-  
14198.
- 23 Bayer, T. A., Schafer, S., Simons, A., Kemmling, A., Kamer, T.,  
Tepests, R., Eckert, A., Schussel, K., Eikenberg, O., Sturchler-  
Pierrat, C., Abramowski, D., Staufenbiel, M. and Multhaup, G.,  
Dietary Cu stabilizes brain superoxide dismutase I activity and  
reduces amyloid A $\beta$  production in APP23 transgenic mice,  
*Proc Natl Acad Sci U S A*, 2003, **100**, 14187-14192.
- 24 Maynard, C. J., Cappai, R., Volitakis, I., Cherny, R. A., White,  
A. R., Beyreuther, K., Masters, C. L., Bush, A. I. and Li, Q. X.,  
Overexpression of Alzheimer's disease amyloid-beta opposes the  
age-dependent elevations of brain copper and iron, *J Biol Chem*,  
2002, **277**, 44670-44676.
- 25 Zheng, H., Jiang, M., Trumbauer, M. E., Sirinathsinghji, D. J.,  
Hopkins, R., Smith, D. W., Heavens, R. P., Dawson, G. R.,  
Boyce, S., Conner, M. W. and et al., beta-Amyloid precursor  
protein-deficient mice show reactive gliosis and decreased  
locomotor activity, *Cell*, 1995, **81**, 525-531.
- 26 von Koch, C. S., Zheng, H., Chen, H., Trumbauer, M.,  
Thinakaran, G., van der Ploeg, L. H., Price, D. L. and Sisodia, S.  
S., Generation of APLP2 KO mice and early postnatal lethality  
in APLP2/APP double KO mice, *Neurobiol Aging*, 1997, **18**,  
661-669.
- 27 Ciccotosto, G. D., Tew, D., Curtain, C. C., Smith, D.,  
Carrington, D., Masters, C. L., Bush, A. I., Cherny, R. A.,  
Cappai, R. and Barnham, K. J., Enhanced toxicity and cellular  
binding of a modified amyloid beta peptide with a methionine to  
valine substitution, *J Biol Chem*, 2004, **279**, 42528-42534.
- 28 Ciccotosto, G. D., Tew, D. J., Drew, S. C., Smith, D. G.,  
Johanssen, T., Lal, V., Lau, T. L., Perez, K., Curtain, C. C.,  
Wade, J. D., Separovic, F., Masters, C. L., Smith, J. P.,  
Barnham, K. J. and Cappai, R., Stereospecific interactions are  
necessary for Alzheimer disease amyloid-beta toxicity,  
*Neurobiol Aging*, 2011, **32**, 235-248.
- 29 Hackett, M. J., McQuillan, J. A., El-Assaad, F., Aitken, J. B.,  
Levina, A., Cohen, D. D., Siegele, R., Carter, E. A., Grau, G. E.,  
Hunt, N. H. and Lay, P. A., Chemical alterations to murine brain  
tissue induced by formalin fixation: implications for  
biospectroscopic imaging and mapping studies of disease  
pathogenesis, *Analyt*, 2011, **136**, 2941-2952.

- 1  
2  
3  
4  
5  
6  
7  
8  
9  
10  
11  
12  
13  
14  
15  
16  
17  
18  
19  
20  
21  
22  
23  
24  
25  
26  
27  
28  
29  
30  
31  
32  
33  
34  
35  
36  
37  
38  
39  
40  
41  
42  
43  
44  
45  
46  
47  
48  
49  
50  
51  
52  
53  
54  
55  
56  
57  
58  
59  
60
- 30 Paterson, D., de Jonge, M. D., Howard, D. L., Lewis, W., McKinlay, J., Starritt, A., Kusel, M., Ryan, C. G., Kirkham, R., Moorhead, G. and Siddons, D. P., The X-ray Fluorescence Microscopy Beamline at the Australian Synchrotron, *AIP Conference Proceedings*, 2011, **1365**, 219-222.
- 31 Ryan, C. G., van Achterbergh, E., Yeats, C. J., Tin Win, T. and Cripps, G., Quantitative PIXE trace element imaging of minerals using the new CSIRO-GEMOC Nuclear Microprobe, *Nucl Instr Meth Phys Res B*, 2002, **189**, 400-407.
- 32 Vogt, S., MAPS: A set of software tools for analysis and visualization of 3D X-ray fluorescence data sets., *J Phys IV*, 2003, **104**, 635-638.
- 33 Brocchieri, L. and Karlin, S., Protein length in eukaryotic and prokaryotic proteomes, *Nucleic Acids Res*, 2005, **33**, 3390-3400.
- 34 Brosnan, J. T. and Brosnan, M. E., The sulfur-containing amino acids: an overview, *J Nutr*, 2006, **136**, 1636S-1640S.
- 35 Pushkar, Y., Robison, G., Sullivan, B., Fu, S. X., Kohne, M., Jiang, W., Rohr, S., Lai, B., Marcus, M. A., Zakharova, T. and Zheng, W., Aging results in copper accumulations in glial fibrillary acidic protein-positive cells in the subventricular zone, *Aging Cell*, 2013, **12**, 823-832.
- 36 Lelie, H. L., Liba, A., Bourassa, M. W., Chattopadhyay, M., Chan, P. K., Gralla, E. B., Miller, L. M., Borchelt, D. R., Valentine, J. S. and Whitelegge, J. P., Copper and zinc metallation status of copper-zinc superoxide dismutase from amyotrophic lateral sclerosis transgenic mice, *J Biol Chem*, 2011, **286**, 2795-2806.
- 37 White, A. R., Reyes, R., Mercer, J. F., Camakaris, J., Zheng, H., Bush, A. I., Multhaup, G., Beyreuther, K., Masters, C. L. and Cappai, R., Copper levels are increased in the cerebral cortex and liver of APP and APLP2 knockout mice, *Brain Res*, 1999, **842**, 439-444.
- 38 Palacios, G., Palacios, J. M., Mengod, G. and Frey, P., Beta-amyloid precursor protein localization in the Golgi apparatus in neurons and oligodendrocytes. An immunocytochemical structural and ultrastructural study in normal and axotomized neurons, *Brain Res Mol Brain Res*, 1992, **15**, 195-206.
- 39 Acevedo, K. M., Hung, Y. H., Dalziel, A. H., Li, Q. X., Laughton, K., Wikke, K., Rembach, A., Roberts, B., Masters, C. L., Bush, A. I. and Camakaris, J., Copper promotes the trafficking of the amyloid precursor protein, *J Biol Chem*, 2011, **286**, 8252-8262.
- 40 Finney, L., Mandava, S., Ursos, L., Zhang, W., Rodi, D., Vogt, S., Legnini, D., Maser, J., Ikpat, F., Olopade, O. I. and Glesne, D., X-ray fluorescence microscopy reveals large-scale relocalization and extracellular translocation of cellular copper during angiogenesis, *Proc Natl Acad Sci U S A*, 2007, **104**, 2247-2252.
- 41 Yang, L., McRae, R., Henary, M. M., Patel, R., Lai, B., Vogt, S. and Fahrni, C. J., Imaging of the intracellular topography of copper with a fluorescent sensor and by synchrotron x-ray fluorescence microscopy, *Proc Natl Acad Sci U S A*, 2005, **102**, 11179-11184.
- 42 Mayer, M. C., Kaden, D., Schauenburg, L., Hancock, M. A., Voigt, P., Roeser, D., Barucker, C., Than, M. E., Schaefer, M. and Multhaup, G., Novel Zinc-binding Site in the E2 Domain Regulates Amyloid Precursor-like Protein 1 (APLP1) Oligomerization, *J Biol Chem*, 2014.
- 43 Zheng, H., Jiang, M., Trumbauer, M. E., Sirinathsinghji, D. J., Hopkins, R., Smith, D. W., Heavens, R. P., Dawson, G. R., Boyce, S., Conner, M. W., Stevens, K. A., Slunt, H. H., Sisoda, S. S., Chen, H. Y. and Van der Ploeg, L. H., beta-Amyloid precursor protein-deficient mice show reactive gliosis and decreased locomotor activity, *Cell*, 1995, **81**, 525-531.
- 44 Wang, Z., Wang, B., Yang, L., Guo, Q., Aithmitti, N., Songyang, Z. and Zheng, H., Presynaptic and postsynaptic interaction of the amyloid precursor protein promotes peripheral and central synaptogenesis, *J Neurosci*, 2009, **29**, 10788-10801.
- 45 Seabrook, G. R., Smith, D. W., Bowery, B. J., Easter, A., Reynolds, T., Fitzjohn, S. M., Morton, R. A., Zheng, H., Dawson, G. R., Sirinathsinghji, D. J., Davies, C. H., Collingridge, G. L. and Hill, R. G., Mechanisms contributing to the deficits in hippocampal synaptic plasticity in mice lacking amyloid precursor protein, *Neuropharmacology*, 1999, **38**, 349-359.
- 46 Yang, L., Wang, B., Long, C., Wu, G. and Zheng, H., Increased asynchronous release and aberrant calcium channel activation in amyloid precursor protein deficient neuromuscular synapses, *Neuroscience*, 2007, **149**, 768-778.